Pairwise interactions of surfactant-covered drops in a uniform electric field

Chiara Sorgentone[1] and Petia M. Vlahovska[2]
[1]*Department of Basic and Applied Sciences for Engineering, Sapienza Università di Roma, 00161 Rome, Italy*
[2]*Engineering Sciences and Applied Mathematics, Northwestern University, Evanston, Illinois 60208, USA*

(Received 2 December 2020; accepted 20 April 2021; published 11 May 2021)

We study the effect of surfactant on the pairwise interactions of drops in an applied uniform dc electric field using a combination of numerical simulations based on a boundary integral formulation and an analytical theory assuming small drop deformations. The surfactant is assumed to be insoluble in the bulk-phase fluids. We show that the surfactant weakens the electrohydrodynamic flow, and thus dielectrophoretic interactions play a more prominent role in the dynamics of surfactant-covered drops compared to clean drops. If drop conductivity is the same as the suspending fluid, a nondiffusing surfactant can arrest the drops' relative motion thereby effectively preventing coalescence.

DOI: 10.1103/PhysRevFluids.6.053601

I. INTRODUCTION

Electric fields are widely used to manipulate particles and fluids. For example, separation of emulsified water from crude oil in the petroleum refining process is achieved by the application of electric fields, which facilitate drop coalescence [1,2]. An important question pertains to the influence of surface-active substances (surfactants, i.e., compounds that lower the surface tension between liquids), which are naturally present in the crude oil (asphaltenes, resins, acids), on the process of droplet attraction and coalescence.

The effect of surfactant (no electric field) has been studied using simulations based on the boundary integral method [3–11], the diffuse-interface-method [12], a front-tracking method [13], or a conserving volume-of-fluid method [14]. The effect of electric fields on clean drops (no surfactant) has been studied theoretically, numerically, and experimentally both for single and multiple drops [15–27], and we refer the interested reader to our recent work [28] for a more extensive bibliography. In that paper, we presented a detailed analysis of the three-dimensional interaction of a drop pair in a uniform electric field. We showed that the pair dynamics are not simple attraction or repulsion; depending on the angle between the center-to-center line with the undisturbed electric field, the relative motion of the two particles can be quite complex. For example, they can attract in the direction of the field and move toward each other, pair up, and then separate in the transverse direction.

The combined effect of surfactants and electric fields is a virtually unexplored problem in terms of numerical experiments, especially when considering multiple drops. This is due to the numerous computational challenges associated with the complex moving geometries and the multiphysics nature of the problem. As a result, numerical simulations are limited to axisymmetric geometries [29,30]. Other theoretical studies developed asymptotic analyses [31–33] to investigate the deformation and the effects of surfactant transport on the deformation of a single viscous drop under a dc electric field.

In this paper, we build upon our previous work [28,34] and explore the effect of an insoluble surfactant on the electrohydrodynamics of a drop pair.

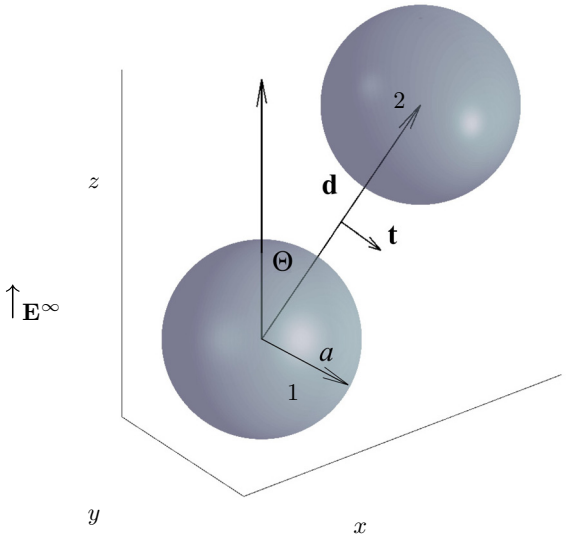

FIG. 1. Two initially spherical identical drops with radius a, permittivity ε_d, and conductivity σ_d suspended in a fluid permittivity ε_s and conductivity σ_s and subjected to a uniform dc electric field $\mathbf{E}^\infty = E_0\hat{\mathbf{z}}$. The angle between the line-of-centers vector and the field direction is $\Theta = \arccos(\hat{\mathbf{z}} \cdot \hat{\mathbf{d}})$.

II. PROBLEM FORMULATION

Let us consider two identical neutrally buoyant and charge-free drops with radius a, viscosity η_d, conductivity σ_d, and permittivity ε_d suspended in a fluid with viscosity η_s, conductivity σ_s, and permittivity ε_s. The mismatch in drop and suspending fluid properties is characterized by the conductivity, permittivity, and viscosity ratios

$$R = \frac{\sigma_d}{\sigma_s}, \quad S = \frac{\varepsilon_d}{\varepsilon_s}, \quad \lambda = \frac{\eta_d}{\eta_s}. \tag{1}$$

A monolayer of insoluble surfactant is adsorbed on the drop interfaces. At rest, the surfactant distribution is uniform and the equilibrium surfactant concentration is Γ_{eq}; the corresponding interfacial tension is γ_{eq}. The distance between the drops' centroids is d, and the angle between the drops' line-of-centers with the applied field direction is Θ. The unit separation vector between the drops is defined by the difference between the position vectors of the drops' centers of mass $\hat{\mathbf{d}} = (\mathbf{x}_2^c - \mathbf{x}_1^c)/d$. The unit vector normal to the drops' line-of-centers and orthogonal to $\hat{\mathbf{d}}$ is $\hat{\mathbf{t}}$. The problem geometry is sketched in Fig. 1.

We adopt the leaky dielectric model [35], which assumes creeping flow and charge-free bulk fluids acting as Ohmic conductors. The assumption of charge-free fluids decouples the electric and hydrodynamic fields in the bulk. Accordingly,

$$\eta\nabla^2\boldsymbol{u} - \nabla p = \mathbf{0}, \quad \nabla \cdot \mathbf{E} = \mathbf{0}, \tag{2}$$

where $\boldsymbol{u}$ and p are the fluid velocity and pressure, and $\mathbf{E}$ is the electric field. Far away from the drops, $\mathbf{E}^s \to \mathbf{E}^\infty = E_0\hat{\mathbf{z}}$ and $\boldsymbol{u} \to \mathbf{0}$.

The coupling of the electric field and the fluid flow occurs at the drop interfaces $\mathcal{D}$, where the charges brought by conduction accumulate. Gauss' law dictates that while the electric field in the electroneutral bulk fluids is solenoidal, at the drop interface the electric displacement field, $\varepsilon\mathbf{E}$, is discontinuous and its jump corresponds to the surface charge density

$$\varepsilon\left(E_n^s - SE_n^d\right) = q, \quad \mathbf{x} \in \mathcal{D}, \tag{3}$$

where $E_n = \mathbf{E}\cdot\mathbf{n}$, and $\mathbf{n}$ is the outward pointing normal vector to the drop interface. The surface charge density adjusts to satisfy the current balance

$$\frac{\partial q}{\partial t} + \nabla_s\cdot(\boldsymbol{u}q) = \sigma_{\rm s}\big(E_n^{\rm s} - RE_n^{\rm d}\big), \quad \mathbf{x}\in\mathcal{D}. \tag{4}$$

In this study, we neglect charge relaxation and convection, thereby reducing the charge conservation equation to continuity of the electrical current across the interface, as originally proposed by [36],

$$E_n^{\rm s} = RE_n^{\rm d}. \tag{5}$$

This simplification implies $\varepsilon_{\rm s}^2E_0^2/(\eta_{\rm s}\sigma_{\rm s}) \ll 1$. This condition is satisfied for the typical fluids used in experiments, such as castor oil (conductivity is $\sim 10^{-11}$ S/m, viscosity is $\sim$1 Pa s), and low field strengths $E_0 \sim 10^4$ V/m.

The electric field acting on the induced surface charge gives rise to electric shear stress at the interface. The tangential stress balance yields

$$(\mathbf{I}-\mathbf{nn})\cdot(\mathbf{T}^{\rm s}-\mathbf{T}^{\rm d})\cdot\mathbf{n} + q\mathbf{E}_t = -\boldsymbol{\nabla}_s\gamma, \quad \mathbf{x}\in\mathcal{D}, \tag{6}$$

where $T_{ij} = -p\delta_{ij} + \eta(\partial_j u_i + \partial_i u_j)$ is the hydrodynamic stress, and δ_{ij} is the Kronecker delta function. The electric tractions are calculated from the Maxwell stress tensor $T_{ij}^{\rm el} = \varepsilon(E_iE_j - E_kE_k\delta_{ij}/2)$. γ is the interfacial tension, which depends on the local surfactant concentration Γ. $\mathbf{E}_t = \mathbf{E} - E_n\mathbf{n}$ is the tangential component of the electric field, which is continuous across the interface, and $\mathbf{I}$ is the idemfactor. The normal stress balance is

$$\mathbf{n}\cdot(\mathbf{T}^{\rm s}-\mathbf{T}^{\rm d})\cdot\mathbf{n} + \tfrac{1}{2}\Big(\big(E_n^{\rm s}\big)^2 - S\big(E_n^{\rm d}\big)^2 - (1-S)E_t^2\Big) = \gamma\,\nabla_s\cdot\mathbf{n}, \quad \mathbf{x}\in\mathcal{D}, \tag{7}$$

where γ is the interfacial tension, which depends on the local surfactant concentration Γ.

The evolution of the distribution of an insoluble, diffusing, charge-neutral surfactant is governed by a time-dependent convective equation [37,38]

$$\frac{\partial\Gamma}{\partial t} + \boldsymbol{\nabla}_{\rm s}\cdot(\boldsymbol{u}_{\rm s}\Gamma) + \Gamma(\boldsymbol{u}\cdot\mathbf{n})\nabla_{\rm s}\cdot\mathbf{n} - D\nabla_s^2\Gamma = 0 \quad \text{at} \quad r = r_s, \tag{8}$$

where $\boldsymbol{\nabla}_{\rm s}$ is the surface gradient operator, $\boldsymbol{\nabla}_{\rm s} = (\mathbf{I}-\mathbf{nn})\cdot\boldsymbol{\nabla}$.

We adopt a linear equation of state for the interfacial tension,

$$\gamma(\Gamma) = \gamma_{\rm eq} - \left.\frac{\partial\gamma}{\partial\Gamma}\right|_{\rm eq}(\Gamma-\Gamma_{\rm eq}). \tag{9}$$

Henceforth, all variables are nondimensionalized using the radius of the undeformed drops a, the undisturbed field strength E_0, a characteristic applied stress $\tau_c = \varepsilon_{\rm s}E_0^2$, and the properties of the suspending fluid. Accordingly, the timescale is $t_c = \eta_{\rm s}/\tau_c$ and the velocity scale is $u_c = a\tau_c/\eta_{\rm s}$. The surfactant concentration is normalized by $\Gamma_{\rm eq}$ and the interfacial tension by $\gamma_{\rm eq}$. The ratio of the magnitude of the electric stresses and surface tension defines the electric capillary number, the relative strength of the distorting viscous and restoring Marangoni stresses is reflected by the Marangoni number, and the importance of surfactant diffusion is given by the Peclet number,

$$\mathrm{Ca} = \frac{\varepsilon_{\rm s}E_0^2a}{\gamma_{\rm eq}}, \quad \mathrm{Ma}^{-1} = \frac{\varepsilon_{\rm s}E_0^2a}{\Delta\gamma}, \quad \mathrm{Pe} = \frac{\varepsilon_{\rm s}E_0^2a^2}{\eta_{\rm s}D}. \tag{10}$$

The characteristic magnitude of the surface-tension variations that result from perturbations of the local surfactant concentration Γ about the equilibrium value $\Gamma_{\rm eq}$ is

$$\Delta\gamma = -\Gamma_{\rm eq}\left(\frac{\partial\gamma}{\partial\Gamma}\right)_{\Gamma=\Gamma_{\rm eq}}.$$

It is convenient to define the elasticity number, which is independent of the externally applied stresses

$$E = \frac{\gamma_0 - \gamma_{\rm eq}}{\gamma_{\rm eq}} = {\rm Ca\,Ma}. \tag{11}$$

III. NUMERICAL METHOD

We utilize the boundary integral method to solve for the flow and electric fields. Details of our three-dimensional formulation can be found in [34]. In brief, the electric field is computed as follows [15,22]:

$$\mathbf{E}^\infty + \sum_{j=1}^{2} \int_{\mathcal{D}_j} \frac{\hat{\mathbf{x}}}{4\pi r^3} (\mathbf{E}^{\rm s} - \mathbf{E}^{\rm d}) \cdot \mathbf{n} dS(\mathbf{y}) = \begin{cases} \mathbf{E}^{\rm d}(\mathbf{x}) & \text{if inside } \mathcal{D}, \\ \frac{1}{2}(\mathbf{E}^{\rm d}(\mathbf{x}) + \mathbf{E}^{\rm s}(\mathbf{x})) & \text{if } \mathbf{x} \in \mathcal{D}, \\ \mathbf{E}^{\rm s}(\mathbf{x}) & \text{if outside } \mathcal{D}, \end{cases} \tag{12}$$

where $\hat{\mathbf{x}} = \mathbf{x} - \mathbf{y}$ and $r = |\hat{\mathbf{x}}|$. The normal and tangential components of the electric field are calculated from the above equation,

$$E_n(\mathbf{x}) = \frac{2R}{R+1} \mathbf{E}^\infty \cdot \mathbf{n} + \frac{R-1}{R+1} \sum_{j=1}^{2} \mathbf{n}(\mathbf{x}) \cdot \int_{\mathcal{D}_j} \frac{\hat{\mathbf{x}}}{2\pi r^3} E_n(\mathbf{y}) dS(\mathbf{y}),$$

$$\mathbf{E}_t(\mathbf{x}) = \frac{\mathbf{E}^{\rm s} + \mathbf{E}^{\rm d}}{2} - \frac{1+R}{2R} E_n \mathbf{n}. \tag{13}$$

For the flow field, we have developed the method for fluids of arbitrary viscosity, but for the sake of brevity here we list the equation in the case of equiviscous drops and suspending fluids. The velocity is given by

$$2\boldsymbol{u}(\mathbf{x}) = -\sum_{j=1}^{2} \left(\frac{1}{4\pi} \int_{\mathcal{D}_j} \left(\frac{\mathbf{f}(\mathbf{y})}{\rm Ca} - \mathbf{f}^E(\mathbf{y}) \right) \cdot \left(\frac{\mathbf{I}}{r} + \frac{\hat{\mathbf{x}}\hat{\mathbf{x}}}{r^3} \right) dS(\mathbf{y}) \right), \tag{14}$$

where $\mathbf{f}$ and $\mathbf{f}^E$ are the interfacial stresses due to surface tension and electric field,

$$\mathbf{f} = \gamma(\mathbf{x}) \mathbf{n} \nabla \cdot \mathbf{n} - \nabla_{\rm s} \gamma, \tag{15}$$

$$\mathbf{f}^E = (\mathbf{E}^{\rm s} \cdot \mathbf{n}) \mathbf{E}^{\rm s} - \tfrac{1}{2} (\mathbf{E}^{\rm s} \cdot \mathbf{E}^{\rm s}) \mathbf{n} - S\big((\mathbf{E}^{\rm d} \cdot \mathbf{n}) \mathbf{E}^{\rm d} - \tfrac{1}{2} (\mathbf{E}^{\rm d} \cdot \mathbf{E}^{\rm d}) \mathbf{n} \big). \tag{16}$$

For a clean drop, the surface tension coefficient $\gamma(\mathbf{x})$ is constant, and the second term in (15), the so-called Marangoni force, vanishes.

Drop velocity and centroid are computed from the volume averages

$$\mathbf{U}_j = \frac{1}{V} \int_{V_j} \boldsymbol{u}\, dV = \frac{1}{V} \int_{\mathcal{D}_j} \mathbf{n} \cdot (\boldsymbol{u}\mathbf{x}) dS, \quad \mathbf{x}_j^c = \frac{1}{V} \int_{V_j} \mathbf{x}\, dV = \frac{1}{2V} \int_{\mathcal{D}_j} \mathbf{n} (\mathbf{x} \cdot \mathbf{x}) dS. \tag{17}$$

To solve the system of equations (13), (14), and (8), we use the Galerkin formulation based on a spherical harmonics representation presented in [34]. In the current study, we update the time scheme to the adaptive fourth-order Runge-Kutta introduced in [39]. This choice allows us to treat the convective term that appears in the surfactant evolution equation (8) explicitly, and the diffusive term implicitly. To make the implicit part of the solver efficient also for large diffusion coefficients (i.e., small Péclet numbers), a preconditioner designed in [40] turns out to be fundamental to reduce the number of iterations for the convergence. All variables (position vector, velocities, electric field, surfactant concentration, etc.) are expanded in spherical harmonics, which provides an accurate representation even for relatively low expansion order. In this respect, to make sure that all the geometrical quantities of interest (e.g., mean curvature) are computed with high accuracy as well,

we use the adaptive up-sampling procedure proposed by [41]. A specialized quadrature method for the singular and nearly singular integrals that appear in the formulation and a reparametrization procedure able to ensure a high-quality representation of the drops also under deformation are used to ensure the spectral accuracy of the method [42].

Our numerical method and the asymptotic theory for clean drops were presented and validated in [28]. Here we extend the small-deformation theory and the numerical method to include the effect of the insoluble surfactant.

IV. THEORY: FAR-FIELD INTERACTIONS

An isolated, charge-neutral drop in a uniform electric field experiences no net force. However, a drop pair moves in response to mutual electrostatic (due to polarization) and hydrodynamic (due to the flow driven by surface electric stresses) interactions.

We first evaluate the electrostatic interaction of two widely separated spherical drops. In this case, the drops can be approximated by point dipoles. The disturbance field $\mathbf{E}_1$ of the drop dipole $\mathbf{P}_1$ induces a dielectrophoretic (DEP) force on the dipole $\mathbf{P}_2$ located at $\mathbf{x}_2^c = d\hat{\mathbf{d}}$, given by $\mathbf{F}(d) = (\mathbf{P}_2 \cdot \nabla \mathbf{E}_1)|_{r=d}$. The drop velocity under the action of this force can be estimated from Stokes' law, $\mathbf{U} = \mathbf{F}/\zeta$, where ζ is the friction coefficient. For a surfactant-covered drop, $\zeta = 6\pi(3\lambda + 2 + \chi)/[3(\lambda + 1) + \chi]$, where $\chi = \mathrm{Pe}\,\mathrm{Ma}$. Thus,

$$\mathbf{U}_2^{\mathrm{dep}} = 2\frac{\beta_D}{d^4}\left(\frac{\chi + 3(1+\lambda)}{\chi + 2 + 3\lambda}\right)[(1 - 3\cos^2\Theta)\hat{\mathbf{d}} - \sin(2\Theta)\hat{\mathbf{t}}], \quad \beta_D = \left(\frac{R-1}{R+2}\right)^2. \tag{18}$$

The velocity reduces to the result for clean drops if $\chi = 0$ [28], and for solid spheres if $\chi \to \infty$.

In addition to the dipole-dipole interaction, drops interact hydrodynamically. Assuming a spherical drop, the electric shear drives a flow, which for an isolated drop is a combination of a stresslet and a quadrupole [36]. This electrohydrodynamic (EHD) flow redistributes the surfactant. The resulting gradients in surface tension (Marangoni stresses) drive a flow. In general, the Marangoni flow further redistributes the surfactant, making the problem nonlinear. However, the feedback can be neglected for small surfactant redistribution, i.e., $\mathrm{Ma}^{-1} \ll 1$, and considering $\Gamma = 1 + \mathrm{Ma}^{-1} g(-1 + 3\cos^2\theta)$. In this case, Marangoni flow has the same symmetry as the flow driven by the electric stresses, and the combined EHD and Marangoni flow outside the drop is

$$\boldsymbol{u} = \frac{\beta}{r^2}(-1 + 3\cos^2\theta)\hat{\mathbf{r}} - \frac{\beta}{r^4}((-1 + 3\cos^2\theta)\hat{\mathbf{r}} + \sin(2\theta)\hat{\theta}), \tag{19}$$

where

$$\beta = \beta_T - \frac{3}{5(1+\lambda)}g, \quad \text{where} \quad \beta_T = \frac{9}{10}\frac{R-S}{(1+\lambda)(R+2)^2}. \tag{20}$$

The surfactant weakens the EHD flow, because the Marangoni stresses due to nonuniform surfactant concentration oppose the shearing electric traction.

If the drops' migration is much slower than the Marangoni timescale, $a/U \ll \eta/(a\Delta\sigma)$, the surfactant distribution reaches steady state, where surfactant convection by the EHD flow is balanced by surfactant diffusion, $\nabla_s \cdot (\boldsymbol{u}\Gamma) = \mathrm{Pe}^{-1}\nabla^2\Gamma$. At leading order, the equation reduces to $\nabla_s \cdot \boldsymbol{u} = -3\,\mathrm{Pe}^{-1}\,\mathrm{Ma}^{-1} g(1 + 3\cos 2\theta)$. Inserting $\boldsymbol{u}$ from Eq. (19) yields

$$g = \chi\frac{5(1+\lambda)}{3[5(1+\lambda)+\chi]}\beta_T, \tag{21}$$

and thus

$$\beta = \frac{9(R-S)}{2(R+1)^2}\frac{1}{5(1+\lambda)+\chi}, \quad \chi = \mathrm{Pe}\,\mathrm{Ma}. \tag{22}$$

Note that the surfactant distribution depends nonlinearly on χ (and thus on Pe). The parameter χ characterizes the magnitude of the surfactant effect on the EHD flow. In the limit $\chi = 0$, the

result reduces to the clean drop solution. In the case of nondiffusing surfactant Pe $\to \infty$ ($\chi \to \infty$), the surfactant completely immobilizes the interface and suppresses the EHD flow, similarly to the problem of a surfactant-covered drop in an applied straining flow [43,44]. In this case, the theory predicts that the drops will interact only electrostatically. Moreover, if $R = 1$, even the DEP interaction vanishes. Thus a pair of spherical droplets covered with insoluble, nondiffusing surfactant and conductivity ratio $R = 1$ will not interact in a uniform electric field.

The drop translational velocity due to a neighbor drop is found from Faxen's law [45,46],

$$\mathbf{U}_2^{\text{ehd}} = \left(1 + \frac{\lambda}{2(3\lambda+2)}\nabla^2\right)\boldsymbol{u}|_{\mathbf{x}=d\hat{\mathbf{d}}}. \tag{23}$$

Inserting Eq. (19) in the above equation leads to

$$\mathbf{U}_2^{\text{ehd}} = \beta\left[\frac{1}{d^2} - \frac{2}{d^4}\left(\frac{1+3\lambda}{2+3\lambda}\right)\right](-1+3\cos^2\Theta)\hat{\mathbf{d}} - \frac{2\beta}{d^4}\left(\frac{1+3\lambda}{2+3\lambda}\right)\sin(2\Theta)\hat{\mathbf{t}} + O(d^{-5}). \tag{24}$$

Combining the electrohydrodynamic and the dielectrophoretic velocities yields

$$\mathbf{U}_2 = \frac{\beta}{d^2}(-1+3\cos^2\Theta)\hat{\mathbf{d}} - \Phi_s(\lambda, R, S, \chi)\frac{2}{d^4}((-1+3\cos^2\Theta)\hat{\mathbf{d}} + \sin(2\Theta)\hat{\mathbf{t}}), \tag{25}$$

where

$$\Phi_s = \frac{1+3\lambda}{2+3\lambda}\beta + \beta_D\frac{3(1+\lambda)+\chi}{2+3\lambda+\chi}. \tag{26}$$

The discriminant Φ_s quantifies the drop pair alignment with the field and the interplay of EHD and DEP interactions in drop attraction or repulsion.

Drops with $\Phi_s > 0$ move to align their line-of-centers with the applied electric field, since $\dot{\Theta} = \mathbf{U}_2 \cdot \hat{\mathbf{t}} \sim -\Phi_s$. If $\Phi_s < 0$ (which occurs only for $R/S < 1$ drops), the line-of-centers between the drops rotates toward a perpendicular orientation with respect to the applied electric field. The presence of surfactant reduces the parameter range where misalignment is predicted. Figure 2 summarizes the regimes of alignment and deformation.

In axisymmetric configurations, $\Theta = 0$ or $\Theta = \pi/2$, the drops' interaction only involves a change in their separation. In a nonaxisymmetric configuration, where the drops' line-of-centers is neither parallel nor perpendicular to the applied field direction, in addition to motions toward or away from each other, the drops' line-of-centers rotate toward or away from the applied field direction. The sign of the EHD and DEP interactions depends on Θ. Equation (18) shows that DEP is attractive only if $\Theta < \Theta_c = \arccos(1/\sqrt{3}) \approx 54.7^\circ$. The EHD interaction also changes sign at Θ_c, as seen from Eq. (24). $R/S < 1$ drops attract if $\Theta < \Theta_c$, and repel otherwise. This scenario is reversed for drops with $R/S > 1$. As a result, as the drops' line-of-centers rotates, the drops' interactions can change from attractive to repulsive or vice versa. Accordingly, the drop trajectories can be quite complex, as illustrated in Fig. 8.

The relative radial motion of the two drops at a given separation depends on Φ_s and β_T. There is a critical separation d_c corresponding to $\mathbf{U}_2(d_c) \cdot \hat{\mathbf{d}} = \mathbf{0}$ at which drop the relative radial motion can change sign,

$$d_c^2 = \frac{2(1+3\lambda)}{2+3\lambda} + \frac{(R-1)^2}{R-S}\left(\frac{4[3(1+\lambda)+\chi][5(1+\lambda)+\chi]}{9(2+3\lambda+\chi)}\right). \tag{27}$$

For $\Phi_s > 0$ and $R/S < 1$ ($\beta < 0$), d_c does not exist, and EHD and DEP interactions are cooperative and act in the same direction (note that a system with $\Phi_s < 0$ and $R/S > 1$ cannot exist). For $\Phi_s > 0$ and $R/S > 1$ or $\Phi_s < 0$ and $R/S < 1$, there is competition between EHD and DEP, with the quadrupolar DEP winning out closer to the drops and the EHD taking over via the stresslet flow in the far-field. The critical distance is affected by the presence of surfactant. It increases with χ, since the surfactant weakens the EHD flow and expands the region of dominance of DEP. In the limit of nondiffusing surfactant, $\chi \to \infty$, the drop interactions are entirely dominated by DEP.

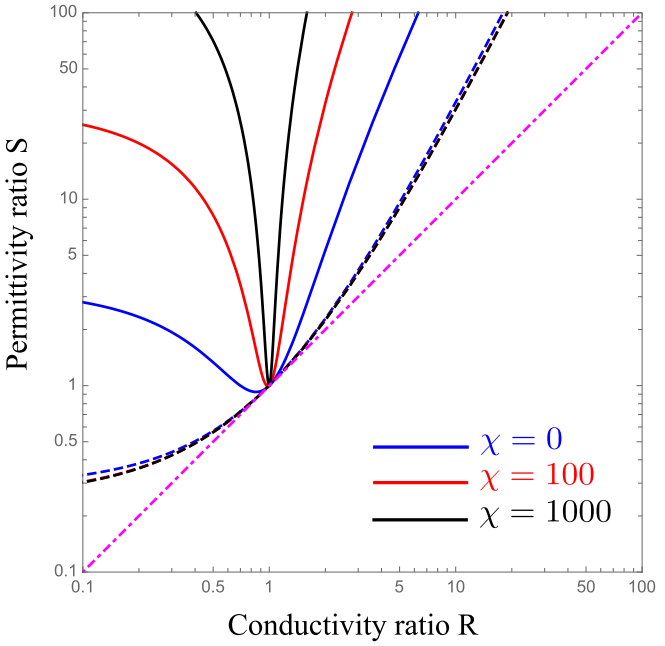

FIG. 2. (a) Phase diagram of drop deformations and alignment with the field for viscosity ratio $\lambda = 1$ and different values of the parameter $\chi = \mathrm{Pe}\,\mathrm{Ma}$. The solid lines correspond to $\Phi_s(\lambda, R, S, \chi) = 0$ given by Eq. (26); in the parameter space above, the line of centers of the two drops rotates away from the applied field direction $\Phi < 0$. The dashed lines correspond to the modified Taylor discriminating function Eq. (A6); in the parameter space above it, drop deformation is oblate, and below it, prolate. Above the dot-dashed magenta line $S = R$, the surface flow is pole-to-equator ($\beta < 0$), while below this line the surface flow is equator-to-pole ($\beta > 0$).

V. RESULTS AND DISCUSSION

We consider two identical drops with viscosity ratio $\lambda = 1$, and we focus on the effect of surfactant on drop dynamics under variable R, S and initial configuration.

First we compare the drop velocity obtained from simulations and the asymptotic theory for a drop pair aligned with the field. After an initial transient, see Fig. 4, drop velocity reaches a nearly steady state. We compare this long-time velocity with the theoretical prediction Eq. (25). Figure 3 shows that theory and simulations are in excellent agreement, especially at large separations, and the theory is able to capture the steady velocity even for a relatively high $\mathrm{Ca} = 1$. As the surfactant effect strengthens and χ increases, either by an increase in the surfactant elasticity or decreasing diffusivity, the drops' relative velocity switches from EHD to DEP dominated at the critical distance given by Eq. (27). Accordingly, the slope dependence on distance changes from d^{-2} to d^{-4}. This is most obvious for the $\chi = 100$ case, where $d_c = 7.14$. In the limit $\chi \to \infty$, the drop motion is entirely due to DEP.

However, even in this limit where the interface is immobilized by the surfactant, until the steady DEP-dominated state is reached, there is EHD affected drop motion due to the transient drop deformation and surfactant redistribution. As a result, the drops can initially repel and then attract once steady drop shape and surfactant distribution are reached. This scenario is illustrated in Fig. 4, which shows that the radial relative velocity in the case of a drop covered with nondiffusing surfactant can change sign from positive (indicating drop repulsion) to negative (attraction). The small-deformation theory that predicts this phenomenon is presented in the Appendixes. Drop deformation and surfactant redistribution are quantified by the parameters D and D_Γ defined as

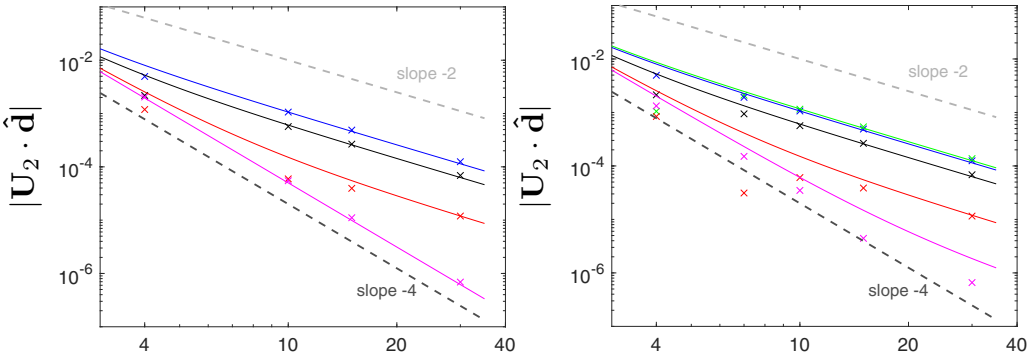

FIG. 3. Steady relative velocity of a pair of leaky dielectric drops aligned with the field ($\Theta = 0$). $R = 2$, $S = 1$, $\mathrm{Ca} = 1$. Left: $E = 1$, $\mathrm{Pe} = 1$ (blue); $\mathrm{Pe} = 10$ (black); $\mathrm{Pe} = 100$ (red); and $\mathrm{Pe} \to \infty$ (magenta). The symbols are from our fully 3D code and the solid line is the theory Eq. (25). In the case of nondiffusing surfactant, the interaction is dominated by DEP and the velocity shows $1/d^4$ dependence. Right: $\mathrm{Pe} = 1$ and $E = 0, 1, 10, 100, 1000$ (green, blue, black, red, magenta). As $\chi = \mathrm{Ma}\,\mathrm{Pe}$ increases, the critical distance beyond which the DEP dominates increases. Note that $\chi = 100$ shows a change of slope from -4 and -2. $\chi = 1000$ slope -4 in the studied range.

$$D = \frac{a_{||} - a_{\perp}}{a_{||} + a_{\perp}}, \quad D_{\Gamma} = \frac{\Gamma_{||} - \Gamma_{\perp}}{\Gamma_{||} + \Gamma_{\perp}}, \tag{28}$$

where $a_{||}$, $a_{\perp}$ and $\Gamma_{||}$, $\Gamma_{\perp}$ are, respectively, the drop lengths and the surfactant concentrations in directions parallel and perpendicular to the applied field.

Our previous study of clean drops [28] found that drops initially misaligned with the field may not experience monotonic attraction or repulsion; instead, their three-dimensional trajectories follow three scenarios: motion in the direction of the field accompanied by either attraction followed by separation or vice versa (repulsion followed by attraction), and attraction followed by separation in a direction transverse to the field. Similar dynamics have been observed with polarizable solid particles undergoing induced-charge electrophoresis as well as dielectrophoretic interactions [47,48]. Surface contamination was found to reduce the strength of ICEP flow [49], similar to the way surfactant suppresses the EHD flow in drops.

Next we address the question about the surfactant influence on these intricate dynamics in the case of drops. The theory presented in Fig. 2 highlighted that the surfactant has two main effects: first, it increases the range of distances where DEP dominates over EHD, and second, it decreases the range of S and R parameters where the drops' line-of-centers rotates away from the direction

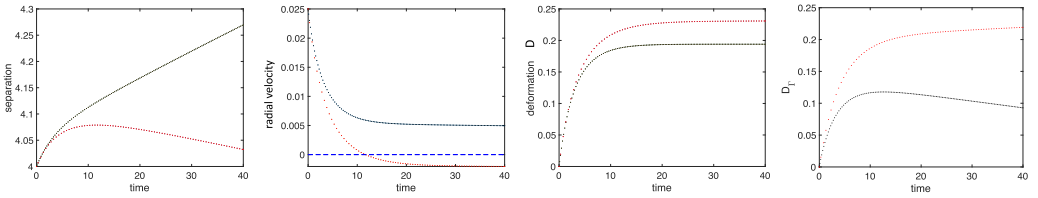

FIG. 4. Effect of surfactant on the interaction of two identical drops with $R = 2$, $S = 1$, $\mathrm{Ca} = 1$, $E = 1$ initially aligned with the field $\Theta = 0$. Black dots correspond to $\mathrm{Pe} = 1$ and red dots correspond to the limit of nondiffusing surfactant $\mathrm{Pe} = 10^6$. The surfactant suppresses the electrohydrodynamic repulsion, and after initial transient due to shape deformation and surfactant redistribution the interaction can reverse sign.

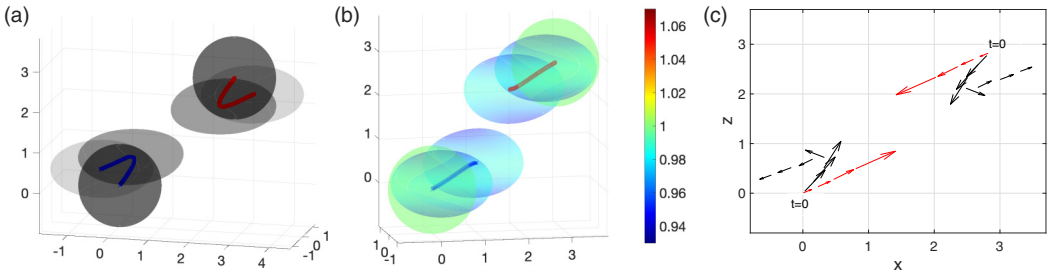

FIG. 5. $R = 0.1, S = 5, \Theta = 45$. Initial distance $d = 4$. (a) Clean drops misaligning, (b) nondiffusing surfactant-covered drops with $E = 10$ aligning with the field, and (c) center-of-mass trajectory in the x-z plane. Arrows correspond to the velocity for the clean drops (black) and for the nondiffusing surfactant-covered drops (red). See the Supplemental Material [50] for the movies.

of the applied field. Accordingly, clean and surfactant-covered drops with the same S and R, initial configuration, and Ca may display opposite aligning behavior. Figure 5 illustrates such a case. While the clean drops attract in the direction of the field and move toward each other, pair up, and then separate in the transverse direction, the surfactant-covered drops only attract and move to align their line-of-centers parallel to the field.

VI. CONCLUSIONS

The effect of surfactant on the three-dimensional interactions of a drop pair in an applied electric field is studied using numerical simulations and a small-deformation theory based on the leaky dielectric model. We present results for the case of a uniform electric field and arbitrary angle between the drops' line-of-centers and the applied field direction, where the nonaxisymmetric geometry necessitates three-dimensional simulations.

The surfactant's main effect is to decrease the electrohydrodynamic flow due to Marangoni stresses compensating the electric shear. As a result, the drops' interactions are more strongly affected by DEP: the surfactant-covered drops tend to align with the applied field direction and attract. The surfactant influence is quantified by the parameter $\chi = \mathrm{Pe}\,\mathrm{Ma}$. The surfactant effect is most pronounced for nondiffusing surfactant ($\mathrm{Pe} \gg 1$) or high elasticity $\mathrm{Ma} \gg 1$. The critical separation at which the DEP overcomes the EHD interaction increases with χ. The interaction is much weaker compared to the clean drops, because DEP decays with the drops' separation as $1/d^4$ compared to the $1/d^2$ for EHD. The DEP also causes drops to align with the field, and the range of R and S where the drops attract and move in the direction of the field and then separate in the transverse direction is greatly diminished.

ACKNOWLEDGMENTS

P.V. has been supported in part by National Science Foundation (NSF) Award No. CBET-1704996.

APPENDIX A: ELECTROHYDRODYNAMIC VELOCITY OF A SURFACTANT-COVERED DROP WITH TRANSIENT DEFORMATION

Let us consider drop dynamics upon the application of a uniform electric field in the limit of small deformations $\mathrm{Ca} \ll 1$. At leading order in Ca, the shape and surfactant concentration are described by $r_s = 1 + f(t)(-1 + 3\cos^2\theta)$ and $\Gamma = 1 + g(t)(-1 + 3\cos^2\theta)$. The shape deformation

parameter is $D = 3f/2$. Combining the small-deformation theories for a surfactant-covered drop in applied flow [51,52] and electric field [53,54] yields

$$\dot{f} = \frac{1}{(3+2\lambda)(16+19\lambda)}[15(1+\lambda)t_n^{\mathrm{el}} + 9(2+3\lambda)t_t^{\mathrm{el}} - \mathrm{Ca}^{-1}\{4f[10(1+\lambda)+E(4+\lambda)] - 2Eg(4+\lambda)\}], \tag{A1}$$

$$\dot{g} = \frac{1}{(3+2\lambda)(16+19\lambda)}[9(2+3\lambda)t_n^{\mathrm{el}} + 9(12+13\lambda)t_t^{\mathrm{el}} - \mathrm{Ca}^{-1}\{12f[2(2+3\lambda) - E(8+7\lambda)] + 6Eg(8+7\lambda)\}] + \mathrm{Pe}^{-1}6(g-2f), \tag{A2}$$

where

$$t_n^e = \frac{1+R^2-2S}{(R+2)^2}, \quad t_t^e = \frac{R-S}{(R+2)^2}. \tag{A3}$$

Steady-state deformation depends on the parameter $\chi = E\,\mathrm{Pe}/\mathrm{Ca} = \mathrm{Pe}\,\mathrm{Ma}$,

$$f = \frac{3\,\mathrm{Ca}}{8}F_S(R,S,\lambda,\chi), \tag{A4}$$

where [31]

$$F_S(R,S,\lambda,\chi) = \frac{1}{(2+R)^2}\left(R^2+1-2S+(R-S)\frac{3(2+3\lambda)+2\chi}{5(\lambda+1)+\chi}\right). \tag{A5}$$

The limit $\chi = 0$ recovers the result for a clean drop $f_{\mathrm{clean}} = 3F_T/8$, where F_T is the Taylor discriminating function

$$F_T(R,S,\lambda) = \frac{1}{(2+R)^2}\left(R^2+1-2S+3(R-S)\frac{2+3\lambda}{5(\lambda+1)}\right). \tag{A6}$$

The limit $\chi \to \infty$ recovers the insoluble surfactant result [32]

$$f = \frac{3}{8}\mathrm{Ca}\frac{(R+1)^2-4S}{(R+2)^2}. \tag{A7}$$

The velocity field outside the drop at distance r from the drop center and an angle θ with the applied field direction is given by [52]

$$\boldsymbol{u} = \left(\frac{\alpha+\beta}{r^2} - \frac{\beta}{r^4}\right)(-1+3\cos^2\theta)\hat{\mathbf{r}} - \frac{\beta}{r^4}\sin(2\theta)\hat{\theta}, \tag{A8}$$

where

$$\alpha = \frac{15(\lambda+1)}{(3+2\lambda)(16+19\lambda)}\left[F_T(R,S,\lambda) - \mathrm{Ca}^{-1}\left(\frac{8}{3}f_2(t) + E\frac{2(4+\lambda)}{15(1+\lambda)}[-2f_2(t)+g_2(t)]\right)\right],$$
$$\beta = \frac{1}{(3+2\lambda)(16+19\lambda)}\left(B_T(R,S,\lambda) - \mathrm{Ca}^{-1}\{12(2+3\lambda)f_2(t) + E(8+7\lambda)[-2f_2(t)+g_2(t)]\}\right), \tag{A9}$$

where

$$B_T(R,S,\lambda) = \frac{9[\lambda(3R^2+13R-19S+3)+2(R^2+6R-8S+1)]}{2(R+2)^2}. \tag{A10}$$

The shape evolution equation is obtained from the kinematic condition $\dot{r}_s = u_r(r=1)$. The surfactant evolution is obtained from $\dot{\Gamma} = -\nabla_s\cdot\boldsymbol{u} + \mathrm{Pe}^{-1}\nabla_s^2\Gamma$.

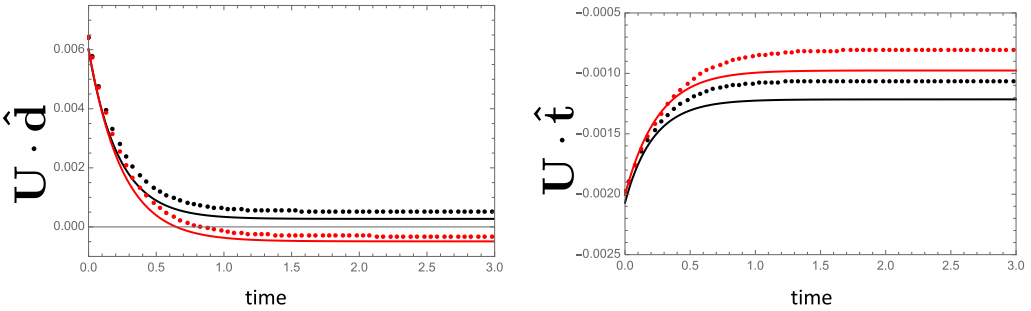

FIG. 6. Evolution of the relative radial (left) and tangential (right) velocities for a drop pair with $R = 2$, $S = 1$. Initial angle $\Theta = 45^\circ$ and distance $d = 4$. Symbols are numerical simulations, and the line is the theory. $\chi = 1$ (black) and $\chi = 10^6$ (red). Note that the relative radial velocity changes sign for $\chi = 10^6$ indicating a change from repulsion to attraction. In both cases, drops move to align their line-of-centers with the applied field direction.

If a second drop is present at location $\mathbf{x}_2^c = d\hat{\mathbf{d}}$, its migration velocity due to the electrohydrodynamic flow of the first drop can be obtained using Faxen's law [45],

$$\mathbf{U}_2^{\text{ehd}} = \left(1 + \frac{\lambda}{2(3\lambda+2)}\nabla^2\right)\boldsymbol{u}(r=d). \tag{A11}$$

Inserting Eq. (A8) in the above equation yields

$$\begin{aligned} U_{2,r}^{\text{ehd}} &= \left[\frac{\alpha+\beta}{r^2} - \frac{1}{r^4}\left(\beta + \frac{3\lambda}{2+3\lambda}(\alpha+\beta)\right)\right](-1+3\cos^2\theta), \\ U_{2,\theta}^{\text{ehd}} &= -\frac{1}{r^4}\left(\beta + \frac{3\lambda}{2+3\lambda}(\alpha+\beta)\right)\sin(2\theta). \end{aligned} \tag{A12}$$

At steady state $\alpha = 0$, and β reduces to the result for a spherical drop Eq. (24).

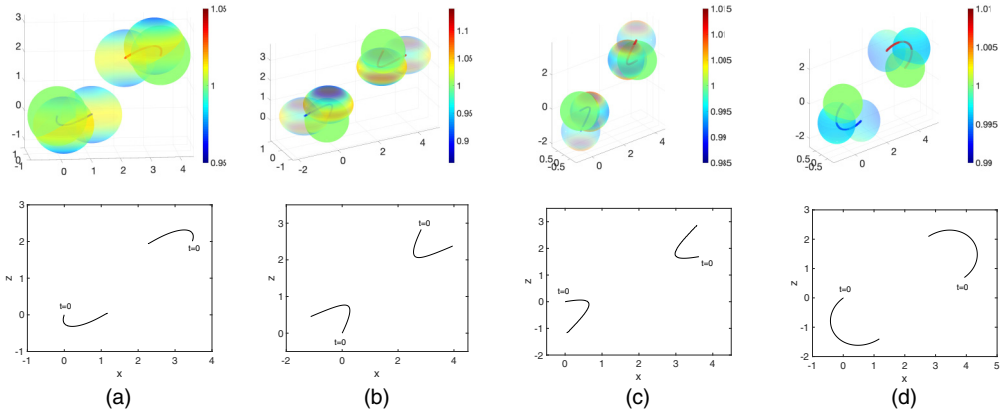

FIG. 7. Trajectories of two identical surfactant-covered drops with (a) $R = 0.1$, $S = 1$; (b) $R = 1$, $S = 10$; (c) $R = 1$, $S = 0.1$; and (d) $R = 100$, $S = 1$. Initially the drops are in the xz plane, the separation in all cases is $d = 4$, and the angle with the applied field direction is (a) $\Theta = 60^\circ$, (b) $\Theta = 45^\circ$, (c) $\Theta = 65^\circ$, and (d) $\Theta = 80^\circ$. Ca $= 0.1$, $E = 1$, and Pe $= 10^6$. Bottom: trajectories in the xz planes. The color map shows the surfactant concentration

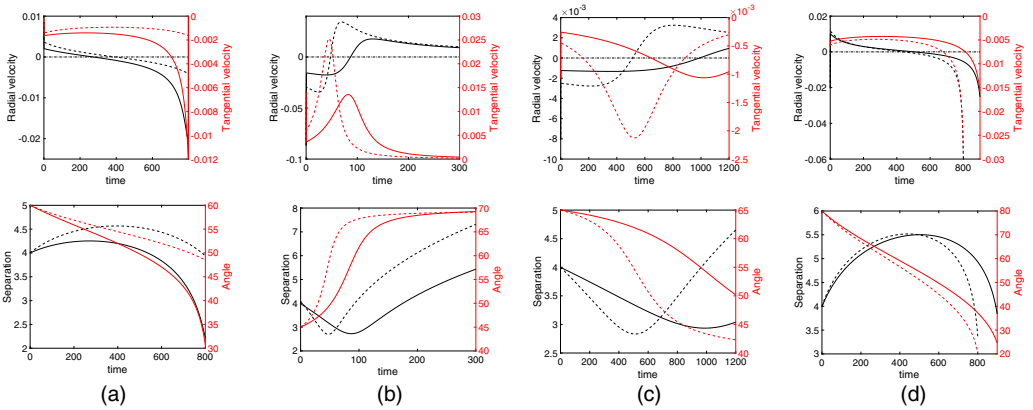

FIG. 8. Dynamics of a pair of identical drops with initial separation $d = 4$ and different angles with the applied field. Comparison between clean (dotted line) and surfactant-covered drops (solid line) with $E = 1$ and $\mathrm{Pe} = 10^6$. $\mathrm{Ca} = 0.1$. (a) $R = 0.1$, $S = 1$ (repulsion-attraction, alignment with the field); (b) $R = 1$, $S = 10$ (attraction-repulsion, misalignment with the field); (c) $R = 1$, $S = 0.1$ (attraction-repulsion, alignment perpendicular to the field); and (d) $R = 100$, $S = 1$ (repulsion-attraction, alignment with the field).

Figure 6 shows the evolution of the radial and tangential velocity and compares the theory with the numerical simulation.

APPENDIX B: 3D TRAJECTORIES OF SURFACTANT-COVERED DROPS IN A UNIFORM ELECTRIC FIELD

Next we illustrate the pair dynamics at different initial configurations. Our previous work showed that clean drops can undergo complex dynamics in an applied uniform electric field if they are initially misaligned with the field: repulsion followed by attraction with centerline rotating toward the applied field direction (a) and (d), attraction followed by repulsion with centerline rotating toward the applied field direction (c), and attraction followed by repulsion with centerline rotating away from the applied field direction (b). The drops remain in the plane defined by the initial separation vector and the applied field direction, in this case the xz plane. The transient pairing dynamics are clearly seen in the trajectories in the xz plane. Figures 7 and 8 show that in these cases, the surfactant does not qualitatively change the dynamics, even though the surfactant concentration does become nonuniform.

[1] L. C. Waterman, Electric coalescers, Chem. Eng. Prog. **61**, 51 (1965).
[2] J. S. Eow and M. Ghadiri, Electrostatic enhancement of coalescence of water droplets in oil: a review of the technology, Chem. Eng. Sci. **85**, 357 (2002).
[3] X. Li and C. Pozrikidis, The effect of surfactants on drop deformation and on the rheology of dilute emulsions in Stokes flow, J. Fluid Mech. **341**, 165 (1997).
[4] C. Pozrikidis, A finite-element method for interfacial surfactant transport, with application to the flow-induced deformation of a viscous drop, J. Eng. Math. **49**, 163 (2004).
[5] H. A. Stone and L. G. Leal, The effects of surfactants on drop deformation and breakup, J. Fluid Mech. **220**, 161 (1990).
[6] S. Yon and C. Pozrikidis, A finite-volume/boundary-element method for flow past interfaces in the presence of surfactants, with application to shear flow past a viscous drop, Comput. Fluids **27**, 879 (1998).

[7] C. D. Eggleton, T. M. Tsai, and K. J. Stebe, Tip Streaming from a Drop in the Presence of Surfactants, Phys. Rev. Lett. **87**, 048302 (2001).
[8] I. B. Bazhlekov, P. D. Anderson, and H. E. H. Meijer, Numerical investigation of the effect of insoluble surfactants on drop deformation and breakup in simple shear flow, J. Coll. Int. Sci. **298**, 369 (2006).
[9] K. Feigl, D. Megias-Alguacil, P. Fischer, and E. J Windhab, Simulation and experiments of droplet deformation and orientation in simple shear flow with surfactants, Chem. Eng. Sci. **62**, 3242 (2007).
[10] P. Vlahovska, J. Bławzdziewicz, and M. Loewenberg, Deformation of a surfactant-covered drop in a linear flow, Phys. Fluids **17**, 103103 (2005).
[11] M. A. Rother, A. Z. Zinchenko, and R. H. Davis, Surfactant effects on buoyancy-driven viscous interactions of deformable drops, Coll. Surf. A **282**, 50 (2006).
[12] K. E. Teigen, P. Song, J. Lowengrub, and A. Voigt, A diffuse-interface method for two-phase flows with soluble surfactants, J. Comput. Phys. **230**, 375 (2011).
[13] M. Muradoglu and G. Tryggvason, A front-tracking method for computation of interfacial flows with soluble surfactants, J. Comput. Phys. **227**, 2238 (2008).
[14] A. J. James and J. Lowengrub, A surfactant-conserving volume-of-fluid method for interfacial flows with insoluble surfactant, J. Comput. Phys. **201**, 685 (2004).
[15] E. Lac and G. M. Homsy, Axisymmetric deformation and stability of a viscous drop in a steady electric field, J. Fluid. Mech. **590**, 239 (2007).
[16] R. B. Karyappa, S. D. Deshmukh, and R. M. Thaokar, Breakup of a conducting drop in a uniform electric field, J. Fluid Mech. **754**, 550 (2014).
[17] J. A. Lanauze, L. M. Walker, and A. S. Khair, Nonlinear electrohydrodynamics of slightly deformed oblate drops, J. Fluid Mech. **774**, 245 (2015).
[18] J. W. Ha and S. M. Yang, Electrohydrodynamics and electrorotation of a drop with fluid less conductive than that of the ambient fluid, Phys. Fluids **12**, 764 (2000).
[19] D. Das and D. Saintillan, Electrohydrodynamics of viscous drops in strong electric fields: numerical simulations, J. Fluid Mech. **829**, 127 (2017).
[20] A. Fernandez, Response of an emulsion of leaky dielectric drops immersed in a simple shear flow: Drops more conductive than the suspending fluid, Phys. Fluids **20**, 043303 (2008).
[21] P. S. Casas, M. Garzon, L. J. Gray, and J. A. Sethian, Numerical study on electrohydrodynamic multiple droplet interactions, Phys. Rev. E **100**, 063111 (2019).
[22] J. C. Baygents, N. J. Rivette, and H. A. Stone, Electrohydrodynamic deformation and interaction of drop pairs, J. Fluid. Mech. **368**, 359 (1998).
[23] Y. Lin, P. Skjetne, and A. Carlson, A phase field model for multiphase electro-hydrodynamic flow, Int. J. Multiphase Flow **45**, 1 (2012).
[24] S. Mhatre, S. Deshmukh, and R. M. Thaokar, Electrocoalescence of a drop pair, Phys. Fluids **27**, 092106 (2015).
[25] P. F. Salipante and P. M. Vlahovska, Electrohydrodynamics of drops in strong uniform dc electric fields, Phys. Fluids **22**, 112110 (2010).
[26] C. Sozou, Electrohydrodynamics of a pair of liquid drops, J. Fluid Mech. **67**, 339 (1975).
[27] M. Zabarankin, Small deformation theory for two leaky dielectric drops in a uniform electric field, Proc. R. Soc. A **476** (2020).
[28] C. Sorgentone, J. I. Kach, A. S. Khair, L. M. Walker, and P. M. Vlahovska, Numerical and asymptotic analysis of the three-dimensional electrohydrodynamic interactions of drop pairs, J. Fluid Mech. **914**, A24 (2021).
[29] K. E. Teigen and S. T. Munkejord, Sharp-interface simulations of drop deformation in electric fields, IEEE Trans. Dielectr. Elec. Insul. **16**, 475 (2009).
[30] H. Nganguia, Y. N. Young, A. T. Layton, W. F. Hu, and M. C. Lai, An immersed interface method for axisymmetric electrohydrodynamic simulations in Stokes flow, Commun. Comput. Phys. **18**, 429 (2015).
[31] J. W. Ha and S. M. Yang, Effects of surfactant on the deformation and stability of a drop in a viscous fluid in an electric field, J. Coll. Int. Sci. **175**, 369 (1995).
[32] H. Nganguia, Y. N. Young, P. M. Vlahovska, J. Blawzdziewcz, J. Zhang, and H. Lin, Equilibrium electrodeformation of a surfactant-laden viscous drop, Phys. Fluids **25**, 092106 (2013).

[33] H. Nganguia, O. S. Pak, and Y.-N. Young, Effects of surfactant transport on electrodeformation of a viscous drop, Phys. Rev. E **99**, 063104 (2019).
[34] C. Sorgentone, A.-K. Tornberg, and P. M. Vlahovska, A 3D boundary integral method for the electrohydrodynamics of surfactant-covered drops, J. Comput. Phys. **389**, 111 (2019).
[35] J. R. Melcher and G. I. Taylor, Electrohydrodynamics - a review of role of interfacial shear stress, Annu. Rev. Fluid Mech. **1**, 111 (1969).
[36] G. I. Taylor, Studies in electrohydrodynamics. I. Circulation produced in a drop by an electric field, Proc. R. Soc. A **291**, 159 (1966).
[37] H. A. Stone, A simple derivation of the time-dependent convective-diffusion equation for surfactant transport along a deforming interface, Phys. Fluids A **2**, 111 (1990).
[38] H. Wong, D. Rumschitzki, and C. Maldarelli, On the surfactant mass balance at a deforming fluid interface, Phys. Fluids **8**, 3203 (1996).
[39] C. A. Kennedy and M. H. Carpenter, Additive Runge-Kutta schemes for convection-diffusion-reaction equations, Appl. Numer. Math. **44**, 139 (2003).
[40] S. Pålsson, C. Sorgentone, and A.-K. Tornberg, Adaptive time-stepping for surfactant-laden drops, in *Eleventh UK Conference on Boundary Integral Methods*, edited by D. J. Chappel (Nottingham Trent University, Nottingham, UK, 2017), pp. 161–170.
[41] A. Rahimian, S. K. Veerapaneni, D. Zorin, and G. Biros, Boundary integral method for the flow of vesicles with viscosity contrast in three dimensions, J. Comput. Phys. **298**, 766 (2015).
[42] C. Sorgentone and A.-K. Tornberg, A highly accurate boundary integral equation method for surfactant-laden drops in 3D, J. Comput. Phys. **360**, 167 (2018).
[43] J. Bławzdziewicz, P. Vlahovska, and M. Loewenberg, Rheology of a dilute emulsion of surfactant-covered spherical drops, Physica A **276**, 50 (2000).
[44] J. Bławzdziewicz, E. Wajnryb, and M. Loewenberg, Hydrodynamic interactions and collision efficiencies of spherical drops covered with an incompressible surfactant film, J. Fluid Mech. **395**, 29 (1999).
[45] S. Kim and S. J. Karrila, *Microhydrodynamics: Principles and Selected Applications* (Butterworth-Heinemann, Stoneham, MA, 1991).
[46] O. S. Pak, J. Feng, and H. A. Stone, Viscous marangoni migration of a drop in a poiseuille flow at low surface peclet numbers, J. Fluid Mech. **753**, 535 (2014).
[47] D. Saintillan, Nonlinear interactions in electrophoresis of ideally polarizable particles, Phys. Fluids **20**, 067104 (2008).
[48] J. S. Park and D. Saintillan, Dipolophoresis in large-scale suspensions of ideally polarizable spheres, J. Fluid Mech. **662**, 66 (2010).
[49] J. S. Park and D. Saintillan, From diffusive motion to local aggregation: Effect of surface contamination in dipolophoresis, Soft Matter **7**, 10720 (2011).
[50] See Supplemental Material at http://link.aps.org/supplemental/10.1103/PhysRevFluids.6.053601 for additional movies showing the effect of surfactant on the drops alignment with the electric field.
[51] P. Vlahovska, J. Bławzdziewicz, and M. Loewenberg, Small-deformation theory for a surfactant-covered drop in linear flows, J. Fluid Mech. **624**, 293 (2009).
[52] P. M. Vlahovska, Dynamics of membrane bound particles: capsules and vesicles, in *Low-Reynolds-Number Flows: Fluid-Structure Interactions*, edited by C. Duprat and H. A. Stone, Royal Society of Chemistry Series RSC Soft Matter (RSC, Cambridge, UK, 2016).
[53] P. M. Vlahovska, On the rheology of a dilute emulsion in a uniform electric field, J. Fluid Mech. **670**, 481 (2011).
[54] P. M. Vlahovska, Electrohydrodynamics of drops and vesicles, Annu. Rev. Fluid Mech. **51**, 305 (2019).